Thermodynamic Properties of a Simple Hard-Core System*

WILLIAM G. HOOVER AND FRANCIS H. REE

Lawrence Radiation Laboratory, University of California, Livermore, California

(Received 9 June 1966)

A simple hard-core system is studied over the entire density range. The model embodies both the simplicity associated with a nearest-neighbor lattice-gas interaction and the realism of a continuous configuration space.

In two dimensions the model system shows no signs of a first-order phase transition. In three dimensions a transition *is* indicated.

I. INTRODUCTION

THE prediction and analysis of phase transitions is the most difficult problem in equilibrium statistical mechanics. Fortunately, the simpler low-density transitions are not sensitive to details of the interparticle potential; thus even crude models with unrealistic potentials can give qualitative or even semiquantitative agreement with experiments. Condensation of gas to liquid, for example, takes place at relatively low density, and even the simplest of all models, the single-occupancy "lattice gas" with nearest-neighbor attractions, has a transition resembling condensation in many respects; the critical compressibility factor for the lattice deviates by only a few percent from that for argon.[1]

The interparticle potential must play a more important role in high-density transitions such as melting. This is evident from the fact that even rather simple materials can exhibit *many* distinct solid–solid phase transitions. The hard-sphere model describes the melting line of argon quite well,[2] while the lattice analog of hard spheres (the nearest-neighbor attractions are replaced by infinite repulsions) has also a phase transition but at a pressure considerably below the hard-sphere transition pressure.[3] This pressure discrepancy is even greater at higher density where the isotherms for hard-core continuum and lattice gases differ in analytic form.[4]

The hard-sphere phase transition has so far been established only by extensive Monte Carlo[5] and molecular dynamic[6] calculations. Existing theories are useful only at densities somewhat higher or somewhat lower than the density range where two phases are thought to coexist. We have been studying in detail a simple *continuum* model, introduced earlier[7] to mimic the hard-sphere system, but more amenable to calculation than hard spheres. The model is described in Sec. II. The potential has a hard core and a continuous configuration space, but the interactions are restricted to nearest neighbors, a simplification borrowed from the lattice gas. One expects that the hybrid nature of the model will yield thermodynamic properties intermediate between those of a hard-core lattice gas and a hard-sphere continuum system. We believe that hard-sphere melting can be represented only with a continuous configuration space. If a lattice space is used, then the high-density solid-phase pressure and entropy differ in analytic form from those of hard spheres.

We began our investigation of the model system in two dimensions. Calculation and analysis of grand partition functions for systems containing up to 25 particles and with three different kinds of boundary conditions strongly suggested the lack of any transition. In view of the evidence for a first-order transition in the similar hard-disk system, this came as something of a surprise. Nevertheless, more elaborate numerical calculations for larger two-dimensional systems confirmed the absence of a melting transition of the hard-disk type for the two-dimensional model.

Next, the three-dimensional model system was studied. Theoretical predictions suggested a strong dependence of the results on dimensionality, and indeed the three-dimensional model differs qualitatively from the two-dimensional model. Two kinds of phases, ordered and disordered, were observed in the three-dimensional calculations, with a transition indicated at about three-fourths the close-packed density.

The two- and three-dimensional data are presented in Secs. III and IV, respectively. These results are discussed and compared with the known hard-disk and hard-sphere results in Sec. V.

* This work was performed under the auspices of the U.S. Atomic Energy Commission.

[1] M. E. Fisher, Phys. Rev. **136**, A1599 (1964).

[2] J. S. Rowlinson, Rept. Progr. Phys. **28**, 169 (1965).

[3] The two-dimensional lattice transition has been studied by L. K. Runnels, Phys. Rev. Letters **15**, 581 (1965); D. S. Gaunt and M. E. Fisher, J. Chem. Phys. **43**, 2840 (1965); F. H. Ree and D. Chesnut, "Phase Transition of a Hard-Core Lattice Gas. The Square Lattice with Nearest-Neighbor Exclusion," J. Chem. Phys. (to be published). The compressibility factor is about $\frac{1}{5}$ that observed in the hard-disk transition by B. J. Alder and T. E. Wainwright, Phys. Rev. **127**, 359 (1962).

[4] W. G. Hoover, B. J. Alder, and F. H. Ree, J. Chem. Phys. **41**, 3528 (1964).

[5] W. W. Wood and J. D. Jacobson, J. Chem. Phys. **27**, 1207 (1957); Proc. Western Joint Computer Conf., San Francisco, 1959, 261 (1959).

[6] B. J. Alder and T. E. Wainwright, J. Chem. Phys. **27**, 1208 (1957); **33**, 1439 (1960).

[7] W. G. Hoover, J. Chem. Phys. **44**, 221 (1966).

II. MODEL SYSTEM

Because the model system has already been discussed,[7] the present description is kept brief. We occasionally specialize to a two-dimensional description and notation, but for the most part the results of this section are given as explicit functions of the number of dimension, D. N particles are confined to a volume V, and that volume is divided up into a network of D-dimensional cubic cells of unit volume. Each cell can be at most singly occupied. Particles in nearest-neighbor cells interact as D-dimensional hard parallel cubes of unit sidelength. It is convenient to introduce an occupation number ω_i for the ith cell, with ω_i equal to 1 when the ith cell is occupied and to 0 if the cell is empty. We indicate an acceptable set of occupation numbers, N ones and $V-N$ zeros, by ω. In Fig. 1 a representative two-dimensional configuration of 15 particles in 49 cells is shown. The second-neighbor overlaps, indicated by heavy shading, distinguish the present model from the hard-parallel-square model where such overlaps are not allowed. It should be noted that the model particles, unlike spheres or cubes, do not really have a definite "shape"—the shape of the excluded volume depends upon where a particle is with respect to the cell boundaries. Although cubes resemble spheres more closely than do the "shapeless" particles of the present model, cubes are not so convenient for high-density calculations.

We can write the configurational integral Q_N as a sum over the $\binom{V}{N}$ sets of occupation numbers ω:

$$Q_N \equiv (N!)^{-1} \int \exp(-\Phi/kT) d\mathbf{r}^N = \sum_\omega Q_N(\omega). \quad (1)$$

The potential energy Φ depends on the coordinates of all the particles $\mathbf{r}^N$; k is Boltzmann's constant, and T is the temperature. The restricted integrals $Q_N(\omega)$ each correspond to a particular distribution of particles in the cells, such as the two-dimensional case shown in the smaller drawing in Fig. 1. In two dimensions, for example, interactions between particles in the same row (column) depend upon their $x(y)$ coordinates only so that $Q_N(\omega)$ separates into a product of one-dimensional integrals:

$$Q_N = \sum_\omega Q_N(\omega) = \sum_\omega q_x(\omega) q_y(\omega). \quad (2)$$

The product form obtained here results directly from the restriction of interactions to particles occupying nearest-neighbor cells. Second-neighbor interactions would couple the x and y integrals. The product form (2) suggests the approximation that the integrals in different directions are not only uncoupled, but also uncorrelated: $\langle q_x(\omega) q_y(\omega) \rangle \equiv \langle q_x q_y \rangle \doteq \langle q_x \rangle \langle q_y \rangle \equiv \langle q \rangle^2$. For the present model it is shown in Sec. III that this approximation is a good one, and therefore is of considerable utility in interpreting results. The re-

sulting thermodynamic properties turn out to be identical with those derived earlier[8] by selecting an infinite set of star integrals from those contributing to the virial expansions of the pressure and entropy. Because of its graphical derivation that approximation was called the "complete-star approximation," and we use the same name here. Most graphical approximations, summing some integrals and ignoring others, have no physical interpretation and are chosen only for mathematical convenience. For the present model the basis of the complete-star approximation *is* physical. Because the implied lack of correlation suggests disorder typical of a *fluid* phase, we expect the approximation to be most useful at low to moderate densities. In fact the complete-star approximation reproduces the first three virial coefficients correctly; this shows its validity at low density.

To calculate thermodynamic properties in the complete-star approximation, one first computes $\langle q \rangle$, the average value of q, from the known one-dimensional configurational integral, $Q_{1-D} = (V-N)^N/N!$. Dividing Q_{1-D} by the number of terms in the sum, $\binom{V}{N}$, one obtains $\langle q \rangle = (V-N)^N (V-N)!/V!$. In D dimensions, the complete-star configurational integral and the
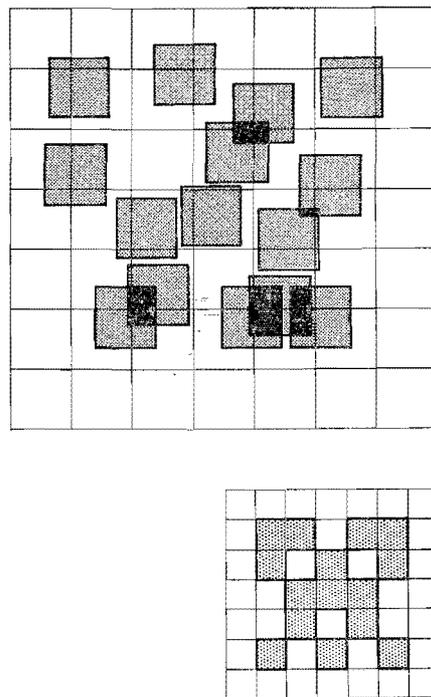

FIG. 1. A configuration of 15 two-dimensional particles in 49 cells. The larger drawing illustrates the diagonal overlaps (heavy shading) which are allowed for this potential. The smaller drawing shows the corresponding lattice configuration. The shaded cells are occupied by particles and have occupation numbers ω_i of unity. Unoccupied cells, for which the ω_i are zero, are not shaded.

[8] See Eq. (10) in the article by F. H. Ree and W. G. Hoover, J. Chem. Phys. **41**, 1635 (1964).

thermodynamic properties derived from it are the following:

$$Q_{stars} = \frac{(V-N)^{DN}[(V-N)!/V!]^{(D-1)}}{N!},$$

$$(S/Nk)_{stars} = D + [(D-1)/\rho]\ln(1-\rho)$$
$$+ \ln[(1-\rho)/\rho],$$

$$(PV/NkT)_{stars} = [D/(1-\rho)] + [(D-1)/\rho]\ln(1-\rho).$$
$$(3)$$

The number density is $\rho (\equiv N/V)$; $S(\equiv k \ln Q_N)$ and $P(\equiv kT \partial \ln Q_N/\partial V)$ are the configurational entropy and pressure. Notice that the complete-star approximation is exact at all densities in one dimension. In two or more dimensions and at high densities near close packing, one might expect the complete-star approximation to fail. At high density, the free volume per particle is the natural expansion parameter, just as is the density ρ at low density. To make it easier to compare exact results for the D-dimensional configurational integral with those of the complete-star approximation (3), we quote here the high-density expansions of the entropy and pressure in the complete-star approximation. The free volume per particle $(V-N)/N$ is denoted by α:

$$(S/Nk)_{stars} = D \ln\alpha + D + (D-1)\alpha \ln\alpha + O(\alpha),$$

$$(PV/NkT)_{stars} = D/\alpha + (D-1)\ln\alpha + D$$
$$+ (D-1)\alpha \ln\alpha + O(\alpha). \quad (4)$$

In the remainder of this section, rigorous upper and lower bounds for the configurational integral in D dimensions are considered. It is shown that the complete-star approximation has the correct high-density form in either one or two dimensions, but not in three or more dimensions.

For the present model it is possible to exhibit the maximum term $\bar{Q} = (\bar{q})^D$ out of the $\binom{V}{N}$ terms which contribute to Q_N. This gives both lower and upper bounds on the configurational integral:

$$(\bar{q})^D < Q_N < (\bar{q})^{D-1}\sum_\omega q(\omega). \quad (5)$$

The explicit form of $\bar{q}$ is given in Ref. 7. Near close packing, α is small and the inequalities (5) have the form:

$$D \ln\alpha + D + \tfrac{1}{2}D\alpha \ln\alpha + O(D\alpha) < S/Nk < D \ln\alpha$$
$$+ D + \tfrac{1}{2}(D-1)\alpha \ln\alpha + O(D\alpha), \quad (6)$$

where S is the configurational entropy, $k \ln Q_N$. Notice that $(S/Nk)_{stars}$ lies, at high density, below the lower bound in three or more dimensions. We expect, but have not shown, that Q_{stars} is actually a lower bound on Q_N at all densities. The upper bound (5) can be

improved slightly by using the Cauchy-like inequality,[9]

$$Q_N < \sum_\omega [q_x(\omega)]^P \equiv Q_{upper}.$$

This improved bound has the same high-density form as is shown in (6). Because Q_{upper}, unlike the bound (5), is an analytic function and useful over the entire density range, we quote the result in full[10]:

$$\left(\frac{S}{Nk}\right)_{upper} = \alpha \ln\sum_{j=0}^\infty (j!)^{-D}y^j - \ln y \equiv \alpha \ln F_D - \ln y,$$

$$(S/Nk)_{upper} \equiv (1/N)\ln Q_{upper},$$

$$\alpha = \sum_{j=0}^\infty (j!)^{-D}y^j \Big/ \sum_{j=0}^\infty j(j!)^{-D}y^j$$
$$= d \ln y/d \ln F_D. \quad (7)$$

In (7), y is a parameter introduced in the Lagrange-multiplier evaluation of Q_{upper}. F_D is a generalized hypergeometric function[11] satisfying the differential equation,

$$(d/dy)(y\,d/dy)^{D-1}F_D = F_D. \quad (8)$$

At low density, the series expansions in (7) can be used. At high density, an asymptotic solution to (8) can be obtained by expanding $\ln F_D$ in powers of $y^{1/D}$. One finds in this way

$$\ln F_D = Dy^{1/D} - \tfrac{1}{2}(D-1)\ln y^{1/D} - \tfrac{1}{2}(D-1)\ln 2\pi - \tfrac{1}{2}\ln D$$
$$+ \tfrac{1}{24}(D - D^{-1})y^{-1/D} + O(y^{-2/D}). \quad (9)$$

The high-density upper bound on the entropy per particle then follows from (7):

$$S/Nk < (S/Nk)_{upper} = D \ln\alpha + D + \tfrac{1}{2}(D-1)\alpha \ln\alpha$$
$$- [\tfrac{1}{2}(D-1)\ln 2\pi + \tfrac{1}{2}\ln D]\alpha$$
$$- \tfrac{1}{12}D^{-1}(D-1)(D-2)\alpha^2 + O(\alpha^3). \quad (10)$$

An approximate form for the pressure, not a strict bound, can then be obtained by differentiating (10):

$$(P/kT)_{upper} = \frac{\partial(S/Nk)_{upper}}{\partial\alpha} = \ln F_D,$$

$$(P/kT)_{upper} = (D/\alpha) + \tfrac{1}{2}(D-1)\ln\alpha + \tfrac{1}{2}(D-1)$$
$$- \tfrac{1}{2}(D-1)\ln 2\pi - \tfrac{1}{2}\ln D$$
$$- \tfrac{1}{6}D^{-1}(D-1)(D-2)\alpha + O(\alpha^2). \quad (11)$$

[9] See the last inequality on p. 20 of E. F. Beckenbach and R. Bellman, *Inequalities* (Springer-Verlag, Berlin, 1961).

[10] An alternative way to calculate Q_{upper} is to use $(i!)^{-D}$ for z_j in the equations of Sec. II of the paper by L. K. Runnels, J. Chem. Phys. **42**, 212 (1965). Runnels' variables L, B, q, κ, x, and $\bar{x}$ correspond, in our notation, to $V, V, 1, 1, y$, and y, respectively. The thermodynamic properties corresponding to Q_{upper} can then be obtained using Runnels' Sec. III equations for the "Constant Free Length Ensemble." We are grateful to Professor Z. W. Salsburg for pointing out the applicability of Runnels' results.

[11] In one dimension F_D is e^y; in two dimensions F_D is $I_0(2y^{\frac{1}{2}})$, where I_0 is a modified Bessel function.
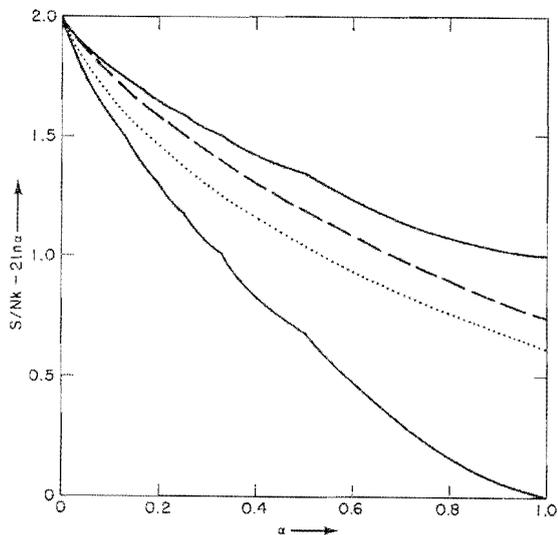
FIG. 2. Entropy for the two-dimensional model system at high density. The variable α is the free volume per particle, $(V-N)/N$, and vanishes at close packing. The heavy full curves are the upper and lower entropy bounds derived by using the maximum term in the partition function. These bounds are given by (5). The dashed line corresponds to the bound $Q_N < \Sigma q^2$, as given by (7). The dotted line corresponds to the complete-star approximation $\langle q_x q_y \rangle \doteq \langle q_x \rangle \langle q_y \rangle$, and lies between the upper and lower bounds at all densities.

In order to compare the predictions of the complete-star approximation with the lower and upper bounds just discussed, the entropy and pressure in two and three dimensions are plotted in Figs. 2 through 5. The entropy upper bound from (10) is better than the upper bound from (5) at all densities. The entropy plots, Figs. 2 and 4, cover the range from $\alpha=0$ (close packing) to $\alpha=1$ (density of half of close packing). The difference between the upper and lower entropy bounds is somewhat smaller in three dimensions than in two. It should be noted that the complete-star approximation entropy agrees well with the results from the various bounds. In two dimensions the complete-star entropy lies neatly between the lower and upper bounds. In three dimensions the situation is different; as the density is increased the complete-star entropy drops below the lower bound at $\rho=0.74879(\alpha=0.33548)$ and the complete-star model is thermodynamically unstable. In more than three dimensions the complete-star model becomes unstable at lower densities, as would be expected for a model describing a disordered phase.

The complete-star isotherms as well as those derived by differentiating the upper bound (7) are shown in Figs. 3 and 5. Notice that the ratio of the pressure in D dimensions to pressure in one dimension is plotted. The complete-star and upper-bound isotherms agree well with one another and suggest that the pressure for the model system lies well below that for more conventional hard-core continuum systems. The hard-

disk and hard-sphere[12] isotherms and parts[13] of the hard-square and hard-cube isotherms are shown for comparison with the model.

In the next two sections exact results and numerical calculations for two- and three-dimensional small systems are described. These indicate the lack of a transition in the two-dimensional case where the disordered complete-star approximation is never unstable and the existence of a transition in three dimensions near the density at which the disordered approximation first becomes unstable.

III. TWO-DIMENSIONAL FINITE SYSTEMS

From preliminary work[7] the model system was known to resemble the hard-sphere system near both ends of the density range. At low density the virial series representation of the pressure is useful and the first five virial coefficients for the model in two or three dimensions lie below those for disks and spheres[14] by
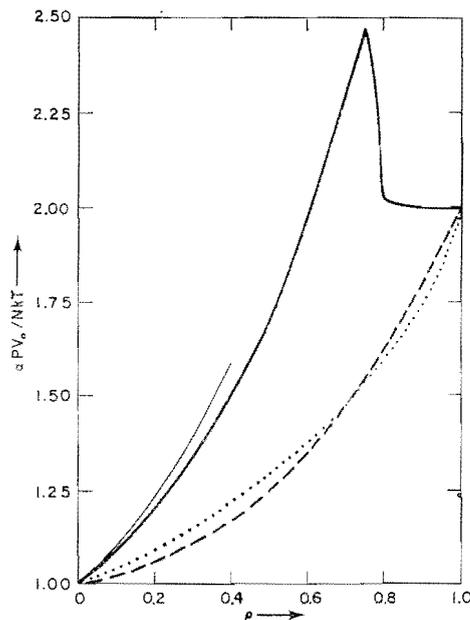

FIG. 3. Ratio of the two-dimensional pressure to the pressure of a one-dimensional hard-rod gas at the same density. V_0 is the close-packed volume. The dashes correspond to the isotherm from (11), obtained by differentiating the entropy upper bound (7). The dots correspond to the complete-star approximation isotherm (3). The known results for disks and squares are also shown for comparison. The hard-disk phase transition corresponds to the steeply decreasing portion of the upper curve.

[12] The position of the hard-sphere phase transition is still unknown so that the tie-line for spheres is not shown in Fig. 5. The density of the solid phase at the transition is probably at least 7/10 the close-packed density.

[13] For squares and cubes, virial coefficients given in the article by W. G. Hoover and A. G. De Rocco, J. Chem. Phys. 36, 3141 (1962) were used.

[14] N. Metropolis, A. W. Rosenbluth, M. N. Rosenbluth, A. H. Teller, and E. Teller, J. Chem. Phys. 21, 1087 (1953); F. H. Ree and W. G. Hoover, ibid. 40, 939 (1964); S. Katsura and Y. Abe, ibid. 39, 2068 (1963); J. S. Rowlinson, Proc. Roy. Soc. (London) A279, 147 (1964).

no more than 20%. The virial coefficients are compared in Table I. At high density too, where the virial series is not useful, the model resembles hard spheres. Both systems[15] are known to have the same D-dimensional limiting form for the entropy per particle, $S/Nk = D\ln\alpha + O(1)$.

These similarities at low and high density suggested that a search for the analog of the hard-sphere phase transition be undertaken. It was expected, based on
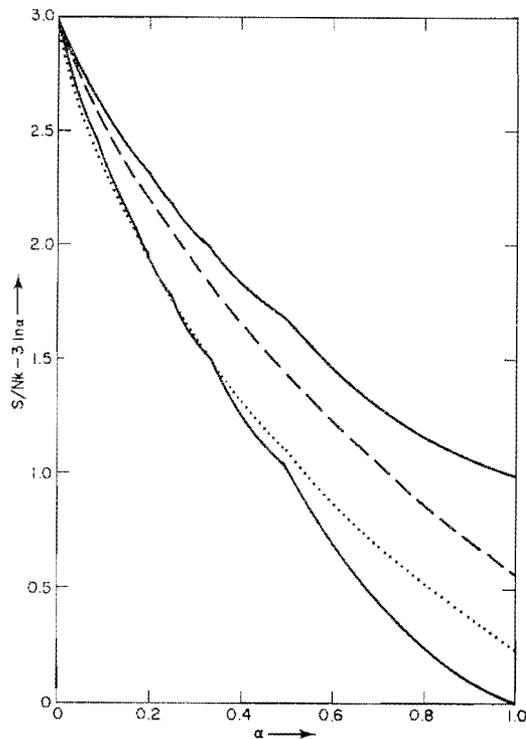

FIG. 5. Ratio of the three-dimensional pressure to the pressure of a one-dimensional hard-rod gas at the same density. V_0 is the close-packed volume. The dots correspond to the isotherm from the upper bound (11). The dashes correspond to the complete-star approximation (3). The known results for spheres and cubes are included, but a tie-line for the hard-sphere transition is not shown because the location of that transition is at present uncertain.

FIG. 4. Entropy for the three-dimensional model system at high density. The variable α is the free volume per particle, $(V-N)/N$, and vanishes at close-packing. The heavy curves were derived from (5) and have discontinuous slopes at densities of $\frac{1}{2}$, $\frac{2}{3}$, $\frac{3}{4}$, $\cdots$, where the analytic form of the bounds changes. The dashed line corresponds to the upper bound $Q_N < \Sigma q^3$. The dots show the entropy according to the complete-star approximation, $\langle q_x q_y q_z \rangle \doteq \langle q_x \rangle \langle q_y \rangle \langle q_z \rangle$. The complete-star approximation breaks down in three dimensions at high density. As the density is increased the entropy according to that approximation first drops below the lower bound at $\alpha = 0.33548$ ($\rho = 0.74879$).

experience[3] with other hard-core systems, that signs of a first-order phase transition could be recognized relatively easily, even in small systems. The choice of ensemble and boundary conditions is particularly important for small systems, and we felt that the

possibility of using several kinds of boundary conditions would give greater insight into the melting transition.

Because the volume, or number of cells, in the model system is an integer it is necessary to use the grand partition function, $\Xi_V = \sum Q_N z^N$. The simplicity of the calculations for the model system compensates for the drawback that phase transitions are not so easily recognized in the grand ensemble.

Because each linear group of k adjacent particles, succeeded and preceded by unoccupied cells, contributes a factor of $(k!)^{-1}$ to the restricted configurational integral $Q_N(\omega)$, it is a simple matter to evaluate these integrals and add them up for sufficiently small V.

[15] The proof for a finite periodic system of spheres is given in the article by Z. W. Salsburg and W. W. Wood, J. Chem. Phys. **37**, 798 (1962). An estimate of the term of order unity is given in the article by F. H. Stillinger, Z. W. Salsburg, and R. L. Kornegay, *ibid.* **43**, 932 (1965). Another estimate for this term, based on integration of the dynamic equation of state (unpublished results of W. G. Hoover and B. J. Alder) leads to a somewhat more positive value for the constant.
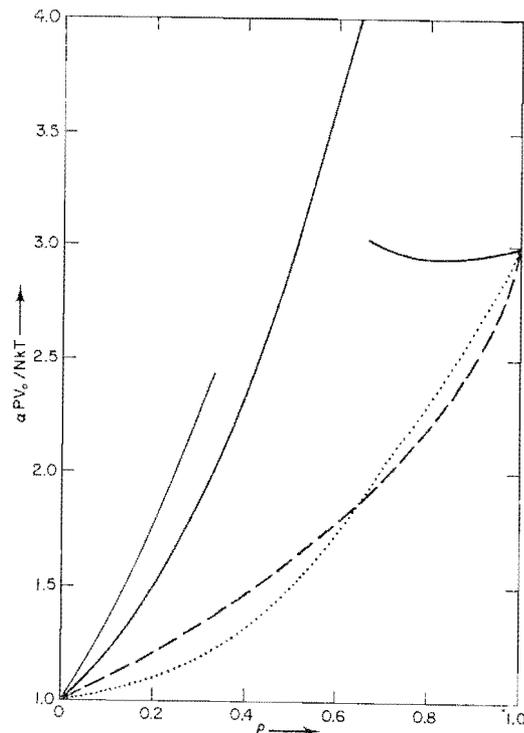
TABLE I. Virial coefficients for hard disks, hard spheres, and the two- and three-dimensional model systems.[a]

	Disks	Spheres	2D Model	3D Model
B_3	0.782	0.625	0.741	0.583
B_4	0.532	0.287	0.463	0.242
B_5	0.334	0.110	0.290	0.100

[a] The coefficients are given in units such that the second virial coefficient is unity for all four systems.
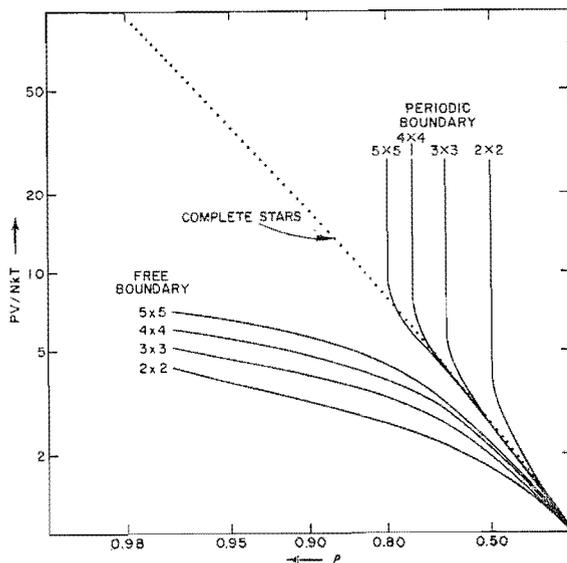
FIG. 6. Compressibility factor PV/NkT as a function of density for systems containing four, nine, 16, and 25 cells. The results in this figure are for both free and periodic boundaries. Note that the latter converge better to the thermodynamic limit. Both scales are logarithmic. The complete-star isotherm (3) has been shown for comparison. In two dimensions this approximation is accurate over the entire density range.

There are 2^V different distributions of from 0 to V particles in V cells so that in practice V must be less than about 30 to obtain analytic results.

Various kinds of boundaries can be used. Our results for three different kinds of boundaries show that for small systems a wise choice is essential. If *free* boundaries are used (a free-boundary system is surrounded by a ring of empty cells as is the set of particles shown in Fig. 1), then the whole density range is accessible but the high-density pressure and entropy will be grossly in error. The small system isotherms obtained with free boundaries are shown in Fig. 6. The pressure is too low at high density.

If free boundaries are used, the entropy per particle approaches $-\ln N$, at close packing rather than $-\infty$.

A more nearly satisfactory choice is periodic boundaries. With periodic boundaries the restricted configurational integral $Q_N(\omega)$ vanishes for any choice of ω giving a completely filled row or column. Thus at the highest density obtainable in the two-dimensional periodic case, there is a single empty cell in each row and each column of the system. In that limit the entropy approaches $2\ln\alpha+2-2.8379\alpha-\cdots$. Although the $\alpha\ln\alpha$ term known from (6) to be present for infinite systems is missing in the periodic-boundary result, there is considerable improvement over the free-boundary result. The periodic-boundary isotherms converge more rapidly to the thermodynamic limit than do the free-boundary isotherms (see Fig. 6).

Helical boundaries were also considered. In the helical case the last cell in each row neighbors the first cell in the next row. The last cell in the last row

completes the chain by neighboring the first cell in the first row. The y direction is treated in the same way. Near close packing, the $\alpha\ln\alpha$ term is also missing for finite helical systems, but the maximum density, $1-V^{-1}$, exceeds that obtainable with periodic boundaries, $1-V^{-1/D}$. The helical-boundary isotherms converge best of all and are shown in Fig. 7.

The partition functions from which the small-system isotherms were derived are listed in the Appendix. As the size of the system is increased, the figures show rapid convergence to the limiting thermodynamic behavior for periodic and helical boundaries except at the highest densities. At the maximum density the pressure incorrectly diverges to infinity logarithmically, just as in the lattice-gas case. At low density it can be shown that the periodic results lie alternately above and below the thermodynamic limit as the sidelength of the system is increased.

Included in Figs. 6 and 7 is the complete-star isotherm. Notice that at all densities up to at least 90% of close packing the finite-system results appear to be converging to a limit quite near to this approximation. The helical boundary results deviate by no more than 5% from the complete-star approximation over this density range.

The "stairstep" character of the high-density part of the helical finite-system isotherms is due to the rapid drop in entropy as density is increased in a continuum system. These same steps are reproduced semiquantitatively if the complete-star isotherms for *finite* systems are calculated. The drop in entropy at high density is much less rapid for a lattice gas. The lattice entropy is zero at close packing, rather than $-\infty$. At high
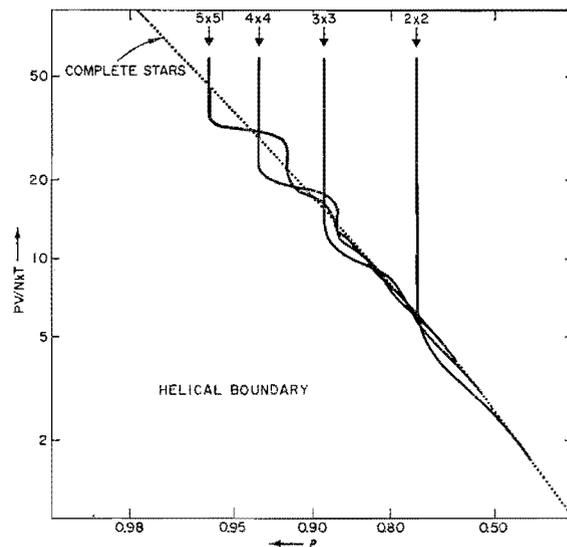

FIG. 7. Compressibility factor PV/NkT as a function of density for systems containing four, nine, 16, and 25 cells with helical boundary conditions. These results extend to higher densities than could be obtained with periodic boundaries. The complete-star isotherm, shown for comparison, is crossed several times by these small-system isotherms.

activity, $z\{\equiv \exp[(PV/NkT)-(S/Nk)]\}$, the small-system grand partition function is essentially given by the two largest terms; the isotherm reflects this two-term structure by approximating an equilibrium pressure between the two densities. As the densities corresponding to adjacent terms in the grand partition function approach each other closely the stairstep effect shifts to higher density. The artificially lumpy isotherm complicates the search for a transition; in particular no significance can be attached to the derivatives of the grand partition function isotherm at high density. These results also show the futility of looking for coefficients in high-density expansions for continuum systems by considering just a few terms in the grand partition function.

Despite the high-density stairstep effect, the convergence for the small system is good enough to rule out the possibility of a bump in the model isotherm of the size observed in hard-disk systems. Lack of a transition is also indicated by the fact that all the zeros of the various two-dimensional partition functions are real. If a transition *were* to occur in the infinite volume limit, then *complex* zeros of the grand partition functions for finite volume would be expected. The qualitative difference between the model and the hard-disk system can best be appreciated by comparing the disk and complete-star isotherms shown in Fig. 3. The disk pressure is much higher in the transition region and in the solid phase.

The results for finite systems of up to 5×5 cells suggest the absence of a phase transition, but to establish this point firmly it was decided to examine larger systems, with periodic boundaries and in the grand ensemble, by using the standard Monte Carlo technique. To assess the size dependence of the results 5×5, 10×10, and 16×16 systems were studied. The agreement of the 5×5 results with those obtained analytically served as a check on the Monte Carlo procedure.

FIG. 9. Compressibility as a function of activity in the two-dimensional model system. The Monte Carlo results show convergence toward the complete-star approximation. There is no sign of a first-order phase transition—such a transition corresponds to an infinite isothermal (reduced) compressibility $\kappa \equiv kT(\partial \ln\rho/\partial P)_T$. $+$, 5×5; O, 10×10; ●, 16×16.

In the Monte Carlo runs, each of the 2^V states of the V-cell system is characterized by a set ω and a statistical weight, $Q_{N(\omega)}z^{N(\omega)}/\Xi_V$. Configurations converging to the grand ensemble distribution were constructed in the usual way.[16] With the system in State i a cell is chosen randomly. Denote the state obtained by changing the occupation number in that cell (i.e., removing or adding a particle) by j. In the event that the weight of State j is greater, the system proceeds to State j. Otherwise, the change is made with probability weight $(i)/\text{weight}(j)$. If the change is not made, the State i is counted again in the chain. This process is repeated until the ensemble averages of the density have converged accurately. The present potential is particularly suited for such a Monte Carlo calculation because the transition probabilities depend only on the states of the row and column in which the cell to be changed lies. The weights associated with all possible configurations of a single row can be stored in the computer (making rows of length 16 about the upper limit, with 2^{16} states).

Two kinds of initial conditions were studied over a wide range of activity. These, an empty lattice and a perfect crystal, both converged rapidly to the same equilibrium density, indicating that the system was never trapped in one of the two maxima to be expected in the density distribution in the case of a first-order phase transition.

The Monte Carlo results (density and isothermal compressibility as a function of activity) are shown in Figs. 8 and 9. The measured values for the largest system appear in Table II. The figures and the table show good agreement with the complete-star approximation. Because a first-order phase transition is associated with an infinite compressibility, the results
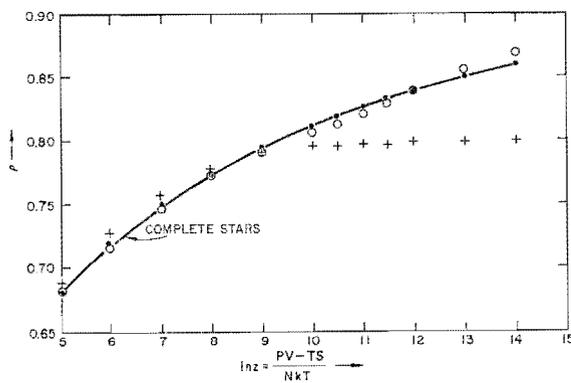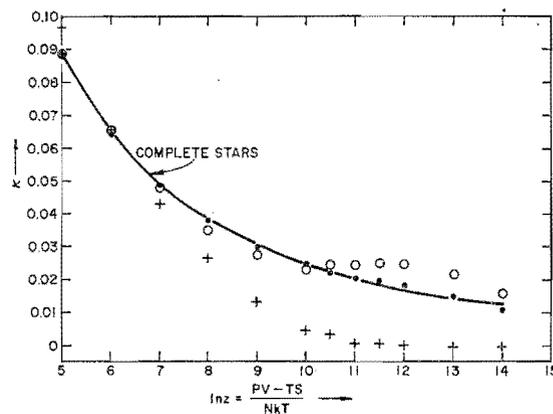

FIG. 8. Density as a function of activity in the two-dimensional model system. These results, obtained by the Monte Carlo method, show rapid convergence toward the complete-star approximation (full curve) as the size of the system is increased from 25 to 256 cells. $+$, 5×5; O, 10×10; ●, 16×16.

[16] See the first paper cited in Ref. 14, and also the article by D. A. Chesnut and Z. W. Salsburg, J. Chem. Phys. **38**, 2861 (1959).

TABLE II. Two-dimensional model system Monte Carlo results (periodic boundaries).[a]

$\ln z$	$\langle \rho \rangle_{MC}$	$\langle \kappa \rangle_{MC}$	ρ_{stars}	$\kappa(\langle \rho \rangle)_{stars}$
5	0.6812	0.0886	0.6798	0.0887
6	0.7174	0.0643	0.7171	0.0648
7	0.7475	0.0491	0.7473	0.0488
8	0.7719	0.0381	0.7722	0.0380
9	0.7926	0.0303	0.7929	0.0303
10	0.8097	0.0249	0.8104	0.0247
10.5	0.8178	0.0225	0.8181	0.0223
11	0.8249	0.0211	0.8253	0.0204
11.5	0.8321	0.0199	0.8319	0.0185
12	0.8388	0.0185	0.8381	0.0168
13	0.8509	0.0151	0.8493	0.0141
14	0.8608	0.0109	0.8591	0.0121

[a] The densities and isothermal (reduced) compressibilities $\kappa \equiv kT(\partial \ln\rho/\partial P)$ were obtained using 1 000 000 configurations in a 16×16 system at various values of the activity $z \equiv \exp[(PV/NkT)-(S/Nk)]$. The values corresponding to the complete-star approximation are given for comparison. The density and compressibility values are accurate to about 0.0005.

in Fig. 9 definitely rule out this possibility. Note from Fig. 9 that the change from 10×10 to 16×16 improves agreement with the complete-star approximation. We conclude that there is no first-order transition for the model in two dimensions.

IV. THREE-DIMENSIONAL FINITE SYSTEMS

In contrast to the two-dimensional case, it is not easy to evaluate analytic grand partition functions for reasonably large three-dimensional systems. It seems likely that a $5\times5\times5$ or $6\times6\times6$ system would have to be worked out analytically to reveal evidence for a hard-sphere-like transition. The limit of what can be done analytically, however, is about $3\times3\times3$. The periodic boundary $2\times2\times2$ case is of some qualitative interest because two of the four zeros of the grand partition function, $\Xi_8 = 1 + 8z + 12z^2 + 8z^3 + 2z^4$, are complex. This, as well as the fact that the complete-star approximation, which corresponds to a disordered phase, is unstable at high density in three or more dimensions, suggests[17] the possibility of a transition.

At first we investigated Monte Carlo configurations for systems $10\times10\times10$ and $16\times16\times16$ in the grand ensemble. The number of configurations which can be generated in a given amount of computer time is not much smaller in three dimensions than in two. In contrast to the two-dimensional results, the density (as a function of activity) obtained in three dimensions *was* dependent on the initial conditions. To sample

[17] See the papers by C. N. Yang and T. D. Lee, Phys. Rev. **87**, 404 (1952).

configuration space adequately, even at rather low values of activity, systems containing no more than $8\times8\times8$ cells should be used.

Just as in two dimensions, the runs started from two different kinds of initial configurations—the empty lattice and the perfect crystal. But, in contrast to two dimensions, the densities obtained after a million configurations typically differed by nearly 1%. That is, the three-dimensional results clearly depended on initial conditions. It was noted that the configurations differed qualitatively as well. At high density and starting from a perfect crystal, the unoccupied cells were found to be equally spaced in the lattice, just as in the maximum-term approximation to the partition function. The configurations generated starting from an empty lattice were characterized by a broad distribution in the spacing of unoccupied cells. This suggests that the two kinds of configurations correspond to two different phases separated by only a small density gap. To judge the relative stability, several runs were made with systems initially containing 50% solid and 50% fluid. This was done by running for 200 000 configurations from an empty start, and then changing the configuration of half the system to that of a perfect crystal. In this way it was determined that for a $10\times10\times10$ system the solid phase is stable at four-fifths the close-packed density and the fluid phase is stable at half the close-packed density. At three-fourths the close-packed density in an $8\times8\times8$ system, the density was found to fluctuate several times between two well-defined plateau values, separated by about 1% in density. Thus, the evidence shows a transition from an ordered to a

TABLE III. Three-dimensional model system Monte Carlo results (periodic boundaries).[a]

$\ln z$	$\langle \rho \rangle_{MC}$	ρ_{stars}
3	0.5065	0.5000
4	0.5606	0.5569
5	0.6076	0.6041
6	0.6464	0.6433
7	0.6781	0.6762
8	0.7046	0.7040
9	0.7266	0.7277
10	0.7462	0.7481
11	0.7625	0.7661
12	0.7768	0.7814
13	0.7897	0.7951
14	0.8027	0.8073

[a] The density values are obtained for a $16\times16\times16$ system starting from an empty lattice. The values given may deviate from true ensemble averages because convergence is quite slow for this size system. The density figures are in any event expected to be accurate within 1%. Compressibility for this system is not meaningful in view of the poor convergence.

disordered phase at roughly three-fourths the close-packed density. This is borne out further by the results obtained by gradually increasing the activity, starting with an empty system in the $16\times16\times16$ case. To determine the high-density expansion parameters, these results (given in Table III) were plotted as in Fig. 10. Note the break in the data at about three-fourths the close-packed density. The plotted data indicate fairly good agreement with the complete-star approximation $\ln[z] = (3/\alpha) - \ln\alpha$ at low density, and a shift to $\ln[z] = (3/\alpha) - 2\ln\alpha - 1$ at high density. Because the data do depend on the initial conditions, we cannot state precise limits on their accuracy.

Although we feel that the present results strongly indicate the presence of a three-dimensional phase transition, present calculator speeds, as well as the dissimilarity of the results to those found for hard disks and hard spheres, suggest it is not worthwhile at present to "locate" this transition more precisely.

V. CONCLUSION

The results found for the model system show a striking difference between two and three dimensions. This is in contrast to the hard-disk and hard-sphere results which indicate order–disorder transitions in both two and three dimensions. It should be kept in mind that the disk and sphere calculations were carried out in the microcanonical ensemble. The number of particles was fixed, and the effect of vacancies on solid phase properties was not studied. In our grand ensemble calculations, vacancies are automatically taken into account. The striking differences between the pressure for the model system and the hard-sphere pressure (which is much higher at intermediate and solid densities) suggest that lattice models with even
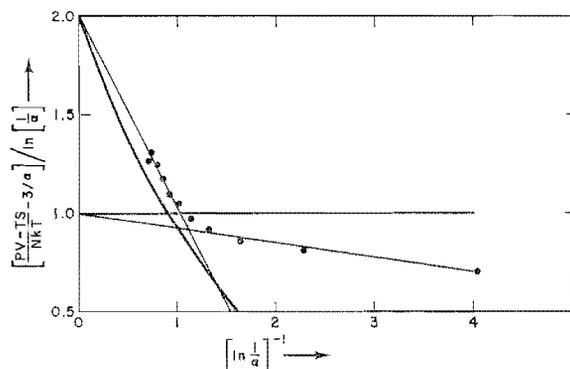

FIG. 10. Plot of the three-dimensional Monte Carlo results for the model system. The heavy curves correspond to the complete-star approximation (horizontal) and the upper bound (7). The known high-density upper and lower bounds suggest that the intercept of the curve must lie between 1.5 and 2.0. The disordered complete-star approximation, which is unstable at high density in three dimensions, has an intercept of 1.0. The two light lines, drawn through the Monte Carlo data points intersect at $(\ln\alpha^{-1})^{-1} \doteq 1.1$, corresponding to a density about three-fourths the close-packed density.

lower pressures, different in analytic form, are not useful in "understanding" the hard-sphere transition.

The fact that the complete-star approximation gives both the high-density and low-density asymptotic forms correctly in one or two dimensions, where no transition was found, but not in three where a transition is indicated, suggests that this approximation may be a useful tool in diagnosing phase transitions. To see whether or not the complete-star approximation would give correctly the high-density hard-disk equation of state, Padé approximations to the hard-disk complete-star isotherm were constructed. These indicate that for disks the complete-star approximation to the pressure diverges as α^{-2} for disks, just as for hard squares, and so is in error at high density. In fact, the complete-star approximation predicts the wrong high-density equation of state not only for hard disks but also for spheres and for a two-dimensional lattice gas known to have a phase transition.[18] It seems likely that the complete-star approximation can describe both high- and low-density properties only in the case that there is no transition linking ordered and disordered phases.

In view of the evidence for the difference in properties of two- and three-dimensional model systems (complete-star approximation, zeros of the grand partition function, two different kinds of configurations in the Monte Carlo runs), it is natural to ask what differences exist between hard disks and hard spheres. A general argument[19] showing the impossibility of an ordered solid phase in two dimensions has been given and is sufficiently general to apply to hard disks. If this argument is valid, then hard disks cannot exhibit long-range order. That is, the correlation between the position of hard disks must vanish at large separations, even at high density. Although it seems quite possible that a solid phase could exist without long-range order there seem to be no definite theoretical results on this question, so that it is a topic worth pursuing.

---

[18] Although it is not accurate at high density, the complete-star approximation does predict condensation in two or more dimensions. For a square-well potential with well width equal to the hard-core diameter, the complete-star approximation $P_{SW}(3-D) \doteq 3P_{SW}(1-D) - 2P$ (ideal lattice gas) predicts a critical compressibility factor about 10% less than that found for argon.

[19] L. D. Landau and E. M. Lifshitz, Statistical Physics (Addison–Wesley Publ. Co., Reading, Mass., 1958), Sec. 125. The extension of the Landau–Lifshitz argument to two dimensions is mentioned in F. H. Stillinger, E. A. DiMarzio, and R. L. Kornegay, J. Chem. Phys. 40, 1564 (1964).

APPENDIX

The two-dimensional finite-system grand partition functions evaluated by direct counting are listed in this Appendix. The results are all expected to be accurate to the number of digits listed.

2×2

	Free	Periodic	Helical
Q_0	1.000000 (0)	1.000000 (0)	1.000000 (0)
Q_1	4.000000 (0)	4.000000 (0)	4.000000 (0)
Q_2	4.000000 (0)	2.000000 (0)	2.500000 (0)
Q_3	1.000000 (0)		1.111111 (−1)
Q_4	6.250000 (−2)		

3×3

	Free	Periodic	Helical
Q_0	1.000000 (0)	1.000000 (0)	1.000000 (0)
Q_1	9.000000 (0)	9.000000 (0)	9.000000 (0)
Q_2	3.000000 (1)	2.700000 (1)	2.725000 (1)
Q_3	4.700000 (1)	3.300000 (1)	3.391667 (1)
Q_4	3.625000 (1)	1.631250 (1)	1.684722 (1)
Q_5	1.325000 (1)	2.812500 (0)	2.711806 (0)
Q_6	2.055556 (0)	9.375000 (−2)	8.668981 (−2)
Q_7	1.284722 (−1)		3.376165 (−4)
Q_8	3.086420 (−3)		5.536069 (−9)
Q_9	2.143347 (−5)		

4×4

	Free	Periodic	Helical
Q_0	1.000000 (0)	1.000000 (0)	1.000000 (0)
Q_1	1.600000 (1)	1.600000 (1)	1.600000 (1)
Q_2	1.080000 (2)	1.040000 (2)	1.042500 (2)
Q_3	4.036667 (2)	3.573333 (2)	3.600000 (2)
Q_4	9.223958 (2)	7.090000 (2)	7.197153 (2)
Q_5	1.343750 (3)	8.360000 (2)	8.568833 (2)
Q_6	1.264660 (3)	5.834444 (2)	6.044940 (2)
Q_7	7.642940 (2)	2.336111 (2)	2.446215 (2)
Q_8	2.900563 (2)	5.040818 (1)	5.326707 (1)
Q_9	6.652076 (1)	5.296639 (0)	5.587623 (0)
Q_{10}	8.724291 (0)	2.457133 (−1)	2.339548 (−1)
Q_{11}	6.084400 (−1)	4.115226 (−3)	2.927331 (−3)
Q_{12}	2.126085 (−2)	1.428898 (−5)	7.051511 (−6)
Q_{13}	3.624433 (−4)		2.875514 (−9)
Q_{14}	2.879192 (−6)		1.757663 (−14)
Q_{15}	9.302722 (−9)		9.356658 (−24)
Q_{16}	9.084689 (−12)		

5×5

	Free	Periodic	Helical
Q_0	1.000000 (0)	1.000000 (0)	1.000000 (0)
Q_1	2.500000 (1)	2.500000 (1)	2.500000 (1)
Q_2	2.800000 (2)	2.750000 (2)	2.752500 (2)
Q_3	1.861000 (3)	1.758333 (3)	1.763250 (3)
Q_4	8.197667 (3)	7.276562 (3)	7.318028 (3)
Q_5	2.532075 (4)	2.055073 (4)	2.074813 (4)
Q_6	5.660440 (4)	4.072622 (4)	4.131444 (4)
Q_7	9.322558 (4)	5.738979 (4)	5.854112 (4)
Q_8	1.141150 (5)	5.769848 (4)	5.921236 (4)
Q_9	1.040406 (5)	4.119509 (4)	4.254227 (4)
Q_{10}	7.041608 (4)	2.063393 (4)	2.144307 (4)

APPENDIX—*Continued*

	Free	Periodic	Helical
5×5			
Q_{11}	3.508729 (4)	7.104085 (3)	7.429098 (3)
Q_{12}	1.270378 (4)	1.630949 (3)	1.717297 (3)
Q_{13}	3.282312 (3)	2.391860 (2)	2.542363 (2)
Q_{14}	5.913462 (2)	2.114858 (1)	2.284163 (1)
Q_{15}	7.219001 (1)	1.050959 (0)	1.162707 (0)
Q_{16}	5.763014 (0)	2.735761 (−2)	3.057250 (−2)
Q_{17}	2.878010 (−1)	3.505929 (−4)	3.617821 (−4)
Q_{18}	8.528901 (−3)	2.016839 (−6)	1.544029 (−6)
Q_{19}	1.425606 (−4)	4.239522 (−9)	1.807934 (−9)
Q_{20}	1.311118 (−6)	1.892644 (−12)	4.013618 (−13)
Q_{21}	6.518617 (−9)		1.852673 (−17)
Q_{22}	1.680636 (−11)		2.257203 (−23)
Q_{23}	2.051323 (−14)		5.397885 (−32)
Q_{24}	1.033636 (−17)		6.494245 (−47)
Q_{25}	1.615056 (−21)		